J. Fluid Mech. (1984), *vol.* 143, *pp.* 69–94
Printed in Great Britain

Two-layer spin-up and frontogenesis

By P. F. LINDEN AND G. J. F. VAN HEIJST†
Department of Applied Mathematics and Theoretical Physics, University of Cambridge, Silver Street, Cambridge CB3 9EW

(Received 9 May 1983 and in revised form 25 January 1984)

The spin-up of a two-layer fluid in a cylinder with a free surface and with a thin lower layer is examined in the laboratory. It is found that when the increase in rotation rate of the cylinder is large enough the radial outflow in the viscous boundary layer on the tank bottom is sufficient to cause the interface to descend near the centre of the tank and to intersect the bottom. The intersection between the interface and the bottom produces a front between stratified (two-layer) fluid and a central region (called the bare spot) in which the upper layer is in direct contact with the bottom. It is observed that the radius of the circular bare spot increases until the lower layer is spun up. Observations of the maximum size of the bare spot are compared with a theoretical calculation in which it is assumed that the lower layer acquires the new angular velocity of the container and where viscous coupling between the layers is neglected. An expansion in F, the upper-layer Froude number, gives good agreement with the observations.

At larger times the circular front is observed to be unstable to frontal waves which appear to gain energy via baroclinic instability from the sloping density interface. At large amplitude these waves 'break', producing regions of closed streamlines in the upper layer. The shape of the bare spot is severely distorted by these waves and the associated motions. The effect of the bottom stress on the spin-up of the upper layer is found to be limited to the bare spot where it is in direct contact with the bottom. Some comments are made on the formation and decay of fronts in the benthic boundary layer of the ocean.

1. Introduction

The response of a fluid in a rotating container to an increase in the rotation rate of the container is a fundamental problem in fluid mechanics. This spin-up problem has received considerable study since the early work of Ekman (1905), and a summary of this work which is still reasonably up to date can be found in Benton & Clark (1974).

The spin-up of a homogeneous fluid in a cylinder rotating about its axis has been described by Greenspan & Howard (1963). They showed that the time taken for the fluid to adjust to the slightly increased rotation rate of the container was $(H^2/\nu\Omega)^{\frac{1}{2}}$, where Ω is the rotation rate of the cylinder, ν the kinematic viscosity of the fluid and H the fluid depth. This timescale is much shorter than the timescale H^2/ν for the viscous diffusion of vorticity from the ends of the cylinder because in the presence of rotation the transfer of stress is essentially advective. The increased rotation rate leads to an increased centrifugal force on the fluid near to the ends of the cylinder which has been viscously accelerated, producing a radial outflow in the fluid adjacent

† Present address: Institute of Meteorology and Oceanography. University of Utrecht, Princetonplein 5, Utrecht, The Netherlands.

to these boundaries. Mass conservation requires that there be a corresponding inflow in the interior of the fluid. This secondary circulation advects rings of fluid towards the axis of rotation which, conserving their angular momentum, increase their angular velocity.

In a stratified fluid the presence of density gradients in the interior of the fluid will affect the secondary circulation which gives rise to the spin-up. For a fluid with a constant vertical density gradient in a cylinder rotating about its (vertical) axis, Walin (1969) showed that spin-up occurs on the same timescale as for a homogeneous fluid, but now the spin-up state is one of non-uniform rotation. On this timescale the vorticity field is rearranged so that there is no differential rotation across the top and bottom Ekman layers. Experiments by Buzyna & Veronis (1971) were in reasonable agreement with these theoretical conclusions.

The spin-up of a two-layer fluid has received relatively little attention, and this is the problem which we shall address here. Our attention was drawn to this problem from a consideration of some oceanographic data, and, in view of the particular configuration we chose to examine, it is worthwhile briefly reviewing the motivation.

Observations of the density structure near the sea bottom over the Hatteras Abyssal Plain (Armi 1978) show that there is often present a benthic boundary layer. This layer is characterised by a vertically well-mixed region extending up from the bottom to a depth of between about 10 m and 50 m and usually capped on the top by a relatively stable pycnocline. In some places the depth of the benthic boundary layer is found to vary abruptly with horizontal position. Such changes in depth were often associated with a benthic front where the capping pycnocline descended and intersected the bottom. This horizontal variability occurs on the scales of tens of km, and Armi & D'Asaro (1980) have suggested that it may result from subsidence produced by the overlying eddy field. When an anticyclonic eddy propagates into a region, the stress exerted by the bottom will cause a divergent flux in the Ekman layer, leading to a thinning of the benthic boundary layer underneath the eddy. If this process is vigorous enough the capping pycnocline will eventually reach the bottom producing a front. This process brings water from above the benthic boundary layer directly in contact with the sea bottom, and provides a mechanism for removing material from the sediments and putting it directly into the water column above the benthic boundary layer. Lambert *et al.* (1983) have invoked this mechanism to explain some of the anomalous vertical distributions of radon 222 observed near the bottom in the oceans.

The essential dynamics of this frontogenetic process have been reproduced by considering the spin-up of a two-layer fluid in a circular cylinder rotating about a vertical axis, in which the lower layer is much shallower than the upper layer. The upper surface is free, and so, ignoring any effect of the sidewall, the only stress exerted on the upper layer results from friction at the interface. In the frame of reference of the container after its angular velocity is increased, the flow in both layers is anticyclonic. As in the benthic boundary layer, Ekman suction reduces the depth of the lower layer near the centre of the tank and can cause the interface to intersect the bottom, producing a front.

We have carried out laboratory experiments on this flow, and these are described in §2. A qualitative description of the flow is given in §3. Some theoretical calculations and a comparison between the theory and experiments is given in §§4–7. Some discussion and the main conclusions are given in §8.

Previous experimental work on two-layer spin-up by Holton (1965) and theoretical calculations by Holton (1965) and Pedlosky (1967) considered the case where the two

layers were of comparable depth and where the interface did not intersect the bottom. When the interface thickness was small compared with the Ekman layers Pedlosky showed that the stress was transmitted in a manner very similar to that in a homogeneous fluid, although local variations in layer thickness produced by baroclinic effects produce departures from solid-body rotation. When the interface thickness is larger than the Ekman layers the interfacial stress is much reduced, and the spin-up process has more in common with that of a uniformly stratified fluid.

Holton (see also Baker 1968) observed baroclinic instability of the interface leading to non-axisymmetric motion during spin-up. We also observed the growth of baroclinic waves on the front. These waves are found to be qualitatively and quantitatively similar to instabilities observed on surface fronts (Griffiths & Linden 1981).

2. The experiments

The experiments were conducted in a number of cylindrical perspex tanks of different dimensions. The internal radii of the tanks were 12.1 cm, 14.9 cm, 44.9 cm and 106.7 cm, and they each had a working depth of about 30 cm. In a given experiment one of these tanks was mounted on a rotating turntable, with the axis of the tank coincident with the (vertical) axis of the turntable. The tank was filled with fresh water to the required depth and then spun up until it was in solid-body rotation. The upper surface of the liquid is a free surface.

A second, denser layer of salt solution, usually containing dye for flow visualization, was then carefully added underneath the fresh water. The salt solution was introduced either via a small source covered with sponge rubber on the bottom of the tank or through a circular pipe attached to the wall of the tank at the bottom. In this way the dense fluid was added adjacent to the tank bottom, and spin-up of the lower layer was rapidly achieved. Once the required amount of salt solution had been added the whole system was left (typically for 30–60 min) until both layers were in solid-body rotation (see figure 1*a*).

The rotation rate Ω of the turntable was then increased, and thereafter remained constant at its new value for the duration of the experiment. The increase in rotation rate of the turntable was achieved within one or two seconds, significantly less than one rotation period. The subsequent fluid flow was visualized by the dye in the lower layer and by paper particles floating on the free surface. In some experiments neutrally buoyant particles were introduced into the two layers, and the motion was revealed by these and by dye released from particles of potassium permanganate dropped into the tank. These motions were recorded using still, streak and ciné photography, and most of the quantitative measurements were obtained from the photographic record.

The buoyancy force associated with the density difference $\Delta\rho$ between the two layers is characterized by a reduced gravity $g' = g\,\Delta\rho/\rho$, where g is the gravitational acceleration and ρ the mean density. In these experiments $1 \leqslant g' \leqslant 50$ cm s^{-2}. The depth of the lower layer h_0 was varied from 0.25 to 4.9 cm, that of the upper layer H from 2.0 to 32.1 cm, and their ratio $\delta = h_0/H$ was in the range $0.01 \leqslant \delta \leqslant 0.54$. The Coriolis parameter $f = 2\Omega$ was varied from 0.39 to 4.76 s^{-1}, and the increase Δf in rotation rate in an experiment was $0.04 \leqslant \Delta f/f \leqslant 3.0$.

Since fresh and salt water, which were used as the working fluids, are miscible, surface tension is negligible at the interface between the layers. The kinematic viscosity ν and the molecular diffusivity of salt κ_S are both effectively constant over

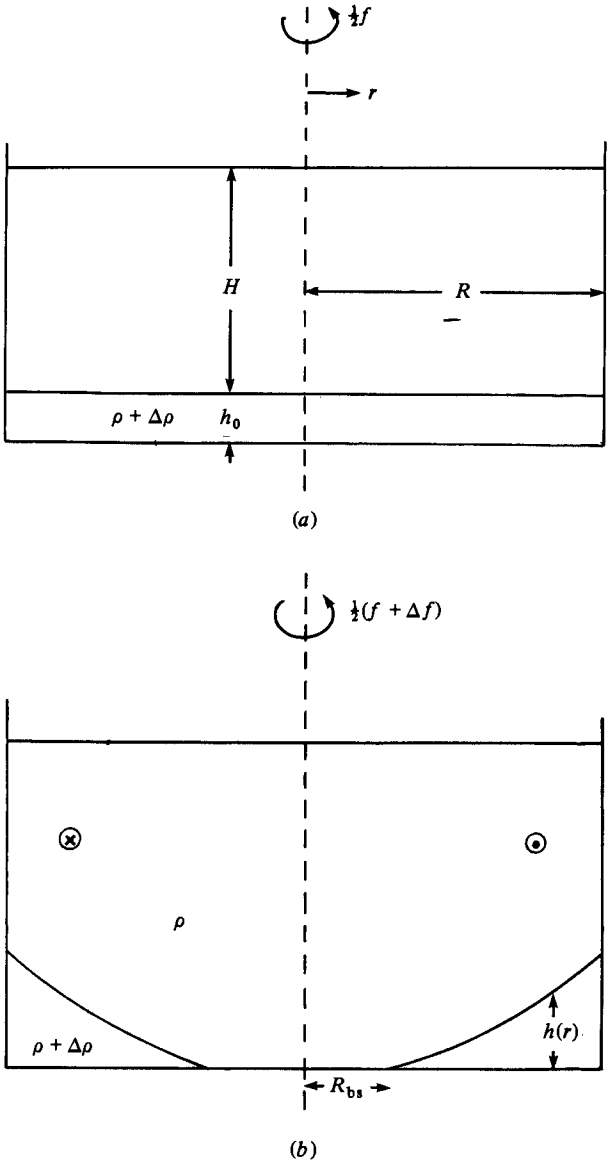

FIGURE 1. Diagrammatic representations of the system before (*a*) and after (*b*) spin-up of the container by an amount $\frac{1}{2}\Delta f$. The situation shown in (*b*) is for the case where Δf is large enough for a 'bare spot' of radius R_{bs} to form during spin-up. The symbols are defined in the text.

the range of concentrations used at 0.01 $cm^2\ s^{-1}$ and 1.5×10^{-5} $cm^2\ s^{-1}$ respectively. In a period of 1 h, therefore, molecular diffusion will have thickened the surface by approximately 0.5 cm. This thickness is comparable to the typical thickness of the interfacial Ekman layer (0.3–0.8 cm). We will return to this point later.

3. A description of the spin-up process

In this section we shall describe the qualitative features of the flow generated during the spin-up of the fluid in the cylinder. Some theoretical considerations and a

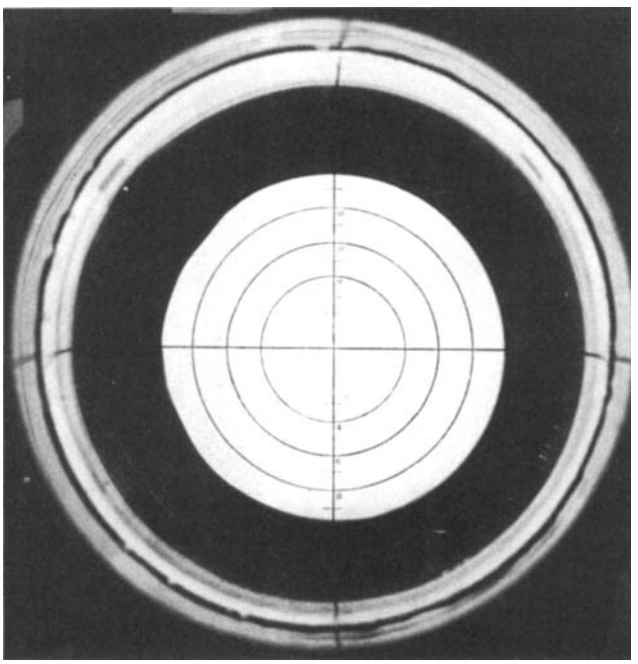

FIGURE 2. An example of the circular 'bare spot' of radius 10 cm, where the clear upper-layer fluid is in contact with the bottom. The dyed lower-layer fluid has been removed from the central region by Ekman-layer suction during spin-up. The edge of the bare spot is a front where the interface between the two layers intersects the bottom. In this experiment $R = 12.1$ cm, $h_0 = 0.6$ cm, $H = 30.0$ cm, $f = 0.81$ s^{-1}, $\Delta f = 2.82$ s^{-1} and $g' = 1.0$ cm s^{-2}. The circular scale on the bottom of the tank is in incremental radii of 2 cm.

quantitative comparison of the theory and the experiments will be given in the following sections.

For the sake of simplicity we first describe the case where the upper layer is very deep and the ratio of layer depths $\delta \ll 1$. The initial response to the increase in rotation rate of the container is for the fluid in the lower layer adjacent to the tank bottom to be (viscously) accelerated. This accelerated fluid experiences an increased centrifugal force which produces a radial outflow in a thin (Ekman) layer near the tank bottom. The effect of this 'centrifugal fan' is to transport fluid outwards, raising the level of the interface at the outer wall and lowering it near the centre of the tank.

If the increase in rotation rate is large enough, the interface will continue to descend and intersect the bottom of the tank. A circular front is thereby produced, marking the boundary between homogeneous (upper layer) fluid on the inside and the two-layer stratification on the outside. If the lower-layer fluid has been dyed, then a plan view reveals the position of the front as the boundary between clear fluid extending to the bottom of the tank in the centre and a ring of dyed fluid as shown on figure 2. The retreat of the lower-layer fluid exposes the tank bottom to the upper-layer fluid: we shall call this exposed region the 'bare spot'.

After some time the radius of the bare spot is observed to stop increasing and the front becomes stationary. During this growth of the bare spot the front remains circular. This situation is depicted schematically in figure 1 (*b*). Viewed in the frame of reference of the container rotating at the new rate $\frac{1}{2}(f+\Delta f)$ the upper layer moves anticyclonically (with an azimuthal velocity given approximately by $-\frac{1}{2}r\,\Delta f$). The

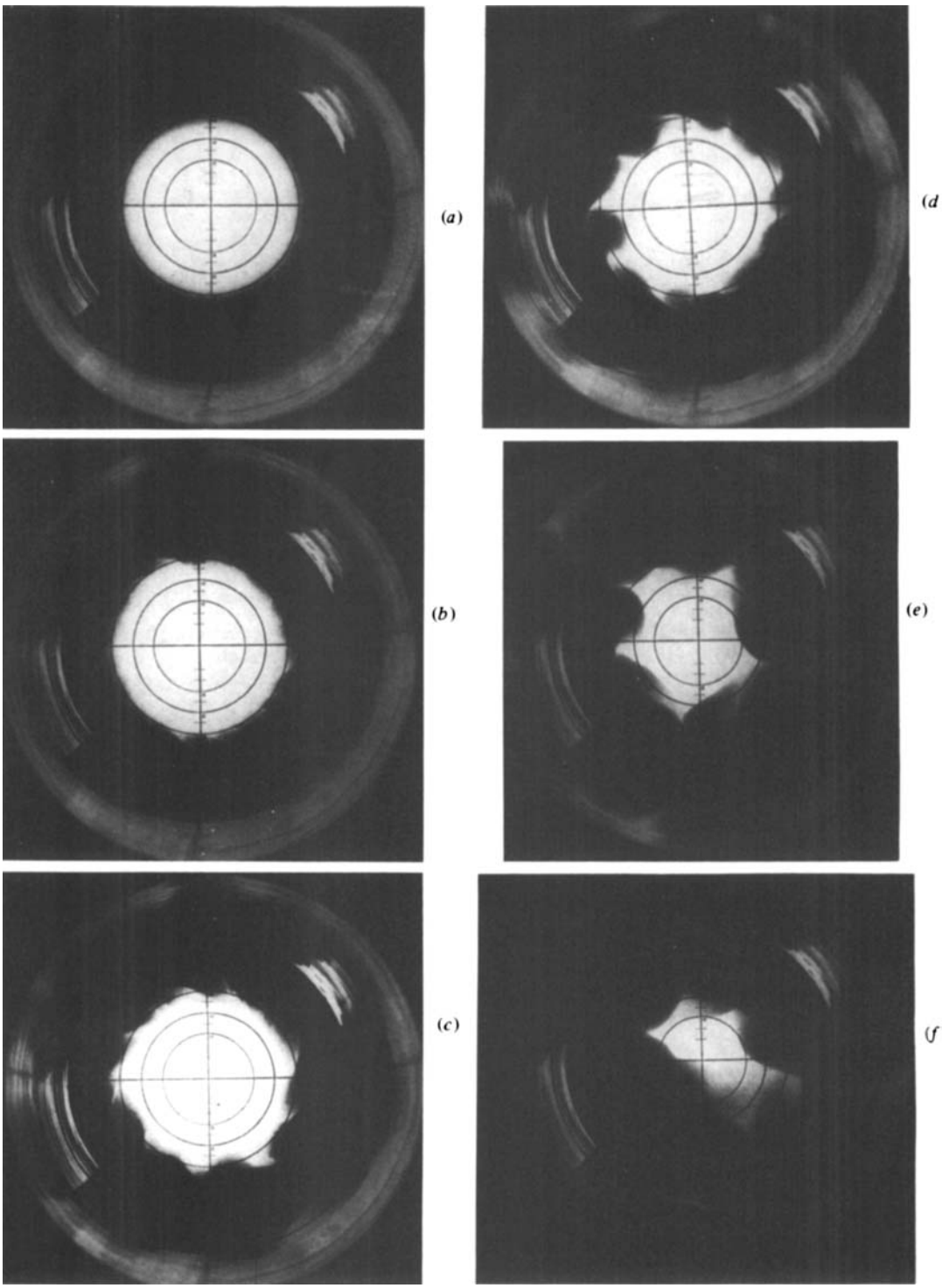

FIGURE 3. A sequence of photographs showing the growth of the frontal waves on the edge of the bare spot. (*a*), taken at 8 rotation periods after spin-up, shows the circular bare spot and evidence of Ekman-layer instability. The photographs (*b*)–(*f*) were taken at approximately 10, 12, 14, 20 and 40 rotation periods after spin-up respectively. The parameter values are $R = 12.1$ cm, $h_0 = 1.0$ cm, $H = 4.0$ cm, $f = 2.67$ s^{-1}, $\Delta f = 2.07$ s^{-1} and $g' = 10$ cm s^{-2}.

lower layer is also observed to move anticyclonically, but at a much slower speed. The vertical shear across the interface is in cyclostrophic balance with the sloping interface.

In some experiments Ekman-layer instability is observed. An example of this instability is shown on figure 3(*a*), where the small-scale striations in the dye associated with the horizontal vortices produced by the instability are clearly visible. These vortices are aligned at a small angle to the flow and have a lengthscale proportional to the Ekman-layer thickness (see e.g. Greenspan 1968, pp. 275–281). These instabilities decay within a few rotation periods as the lower layer spins up.

At larger times wavelike disturbances are observed to grow on the front. An example of the growth and evolution of these unstable waves in the small tank ($R = 12.1$ cm) is shown on figures 3(*b–f*). In this example the frontal waves are beginning to grow (figure 3*b*) in the presence of the Ekman-layer instabilities. On figure 3(*c*), taken some 4 rotation periods later, the Ekman-layer instabilities have decayed and only the frontal waves remain. At this stage the zonal wavenumber is $n = 12$. Large radial excursions of the front are produced by the disturbances as they grow to large amplitude (figures 3*d–e*), and the shape of the bare spot becomes very distorted (figure 3*f*). The waves are observed to propagate anticyclonically, but at a speed intermediate to that of the upper and lower layers. The wavelength of the frontal waves is observed to increase with time. For example, the azimuthal wavenumber n varies from 12 in figure 3(*c*), 10 in 3(*d*) to 7 in 3(*e*), a timespan of 28 rotation periods.

The ultimate state in all the experiments is achieved when both layers acquire the new angular velocity of the tank and the interface takes the shape of the equilibrium parabola appropriate to the increased rotation rate.

During the spin-up, mixing between the two layers sometimes occurs. Mixing was observed to occur more frequently in the larger two tanks where the velocities associated with spin-up of the lower layer were much larger. This mixing produced a thickened interface, but otherwise appeared to have little effect.

4. Theory – infinite upper layer

The formation and growth of the bare spot described in the previous section requires an outward radial flux of lower-layer fluid in the bottom Ekman layer. The cessation of the bare-spot growth can only occur if this Ekman-layer transport is reduced to zero, which would occur if the lower layer were to acquire the new angular velocity of the tank. We shall therefore assume that the ultimate size of the bare spot is obtained when this occurs and the lower layer is spun-up. For the sake of simplicity we shall also assume that the upper layer is infinitely deep ($\delta = 0$) and that there is no interfacial friction.

In the ultimate steady state the azimuthal velocity $v(r)$ and the depth of the lower layer $h(r)$ then satisfy

$$\frac{v^2}{r} + fv = g' \frac{\mathrm{d}h}{\mathrm{d}r}, \tag{4.1}$$

where g' is the reduced gravity, $f = 2\Omega$ is twice the original angular velocity of the tank and r the radial coordinate measured from the axis of rotation. When the lower layer is spun up $v = \frac{1}{2} r \Delta f$, and it is readily seen that

$$h(r) = Ar^2 + B, \tag{4.2}$$

where

$$A = \frac{f^2}{4g'}\left[\frac{\Delta f}{f} + \frac{1}{2}\left(\frac{\Delta f}{f}\right)^2\right]. \tag{4.3}$$

The interface has a parabolic shape with the minimum depth at $r = 0$.

The constant B is determined by conservation of the volume of the lower layer. When the interface does not intersect the bottom ($h(r) \neq 0$, $0 < r < R$) conservation of volume implies

$$2\pi \int_0^R (Ar^2 + B)\, r\, \mathrm{d}r = \pi h_0 R^2,$$

where h_0 is the initial depth of the lower layer and R is the tank radius. Solving this equation for B we find

$$h(r) = h_0 - A(\tfrac{1}{2}R^2 - r^2). \tag{4.4}$$

The interface touches the bottom of the tank if $A = 2h_0/R^2$, and using (4.3) we find

$$\frac{\Delta f}{f} = \left[1 + \frac{16g'h_0}{f^2R^2}\right]^{\frac{1}{2}} - 1. \tag{4.5}$$

For larger values of the incremental increase in rotation rate $\Delta f/f$ than that given by (4.5) the interface will intersect the bottom at $r = R_{\mathrm{bs}}$. Applying the condition $h(R_{\mathrm{bs}}) = 0$ gives $B = -AR_{\mathrm{bs}}^2$, and conservation of volume of the lower layer takes the form

$$2\pi \int_{R_{\mathrm{bs}}}^R A(r^2 - R_{\mathrm{bs}}^2)\, r\, \mathrm{d}r = \pi h_0 R^2.$$

Solving this equation for R_{bs}, we find

$$\frac{R_{\mathrm{bs}}}{R} = \left[1 - \frac{1}{R}\left(\frac{2h_0}{A}\right)^{\frac{1}{2}}\right]^{\frac{1}{2}}. \tag{4.6}$$

This result is the main quantitative prediction of the theory, and will be compared with the experimental predictions.

The timescale for the initial appearance of the bare spot can be estimated from the radial flux Q carried in the Ekman layer. This flux is well known to be (Greenspan 1968)

$$Q = -\tfrac{1}{2}v_1 \delta_{\mathrm{E}}, \tag{4.7}$$

where $\delta_{\mathrm{E}} = [2\nu/(f + \Delta f)]^{\frac{1}{2}}$ is the thickness of the Ekman layer, and v_1 is the velocity of the interior fluid (i.e. the lower layer) relative to the increased rotation rate of the container $\frac{1}{2}(f + \Delta f)$. Taking $v_1 = -\frac{1}{2}r\Delta f$, we get

$$Q = r\Delta f\left[\frac{\nu}{2(f + \Delta f)}\right]^{\frac{1}{2}}. \tag{4.8}$$

Conservation of mass of the lower layer then gives

$$\frac{\mathrm{d}h}{\mathrm{d}t} = \Delta f\left[\frac{\nu}{2(f + \Delta f)}\right]^{\frac{1}{2}}. \tag{4.9}$$

An estimate of the timescale τ for the formation of the bare spot can be obtained by writing $\mathrm{d}h/\mathrm{d}t \sim h_0/\tau$. Then from (4.9) we have

$$\tau = \frac{h_0}{\Delta f}\left[\frac{2(f + \Delta f)}{\nu}\right]^{\frac{1}{2}}. \tag{4.10}$$

The assumption that the lower layer is spun up requires that an ageostrophic radial pressure gradient is set up to provide a small radial inflow throughout the lower layer. This radial pressure gradient is established by inertia–gravity waves which propagate

inwards from the outer boundary of the tank. For long waves with wavelength $\lambda = 2\pi/k \gg h_0$, the group velocity C (see Lighthill 1978, pp. 441–442) is given by

$$C = \frac{g'h_0 k}{(f^2 + g'h_0 k^2)^{\frac{1}{2}}}. \tag{4.11}$$

The time T_w taken for information to propagate from the boundary to the centre of the tank is

$$T_w = \frac{R}{C} = \frac{R(f^2 + g'h_0 k^2)^{\frac{1}{2}}}{g'h_0 k}. \tag{4.12}$$

These waves are dispersive with the shortest wave travelling fastest. For wavelengths comparable or shorter than the Rossby radius of deformation $\mathscr{R} = (g'h_0)^{\frac{1}{2}}/f$, an adequate approximation to the travel time (4.12) is

$$T_w \approx \frac{R}{(g'h_0)^{\frac{1}{2}}} \approx \frac{R}{f\mathscr{R}}. \tag{4.13}$$

Note that this estimate is independent of wavenumber k.

In most of the experiments $\mathscr{R} \ll R$, and so T_w is several rotation periods. The timescale T_s for the spin-up of an unstratified layer of depth h_0 by Ekman pumping is given by

$$T_s = \frac{h_0}{(\nu f)^{\frac{1}{2}}}. \tag{4.14}$$

The ratio of these two timescales is therefore

$$\frac{T_w}{T_s} = \frac{\nu^{\frac{1}{2}} f^{\frac{1}{2}} R}{g'^{\frac{1}{2}} h_0^{\frac{3}{2}}}. \tag{4.15}$$

When $T_w/T_s \ll 1$ the radial pressure gradient required for spin-up is established very quickly, and so the homogeneous spin-up time T_s sets the timescale for the spin-up of the lower layer. On the other hand, when $T_w/T_s \gg 1$ the time taken for the information to propagate in from the outer boundary is the limiting factor. We note that when $R \to \infty$ the lower layer does not spin up, except by viscous diffusion of vorticity from the bottom boundary.

Thus, although the prediction for the bare-spot radius given in (4.6) may be adequate when $T_w/T_s \ll 1$, we expect the prediction to be inappropriate when $T_w/T_s \gg 1$ and the lower layer does not spin up. In this latter case the fluid in the lower layer will accumulate within a Rossby radius or so of the outer boundary of the tank, and R_{bs} will exceed the prediction given in (4.6). We shall comment further on the spin-up in this limit in §8.

5. Quantitative observations of the spin-up

5.1. *Bare-spot formation*

The calculations presented in §4 provide predictions for the timescale τ for the formation of the bare spot (4.10) and its ultimate radius R_{bs} given by (4.6). The time τ for the initial formation was measured with a stopwatch as the elapsed time from the start of the spin-up until the interface first intersected the tank bottom. The results of these measurements are plotted on figure 4 against the predicted time τ obtained from (4.10). Although the results are somewhat scattered, which is due in part to the difficulty in defining the precise moment when the interface touches the bottom, the observations agree fairly well with the calculations.

The observed ultimate size R_{bs} of the bare spot, non-dimensionalized by the tank

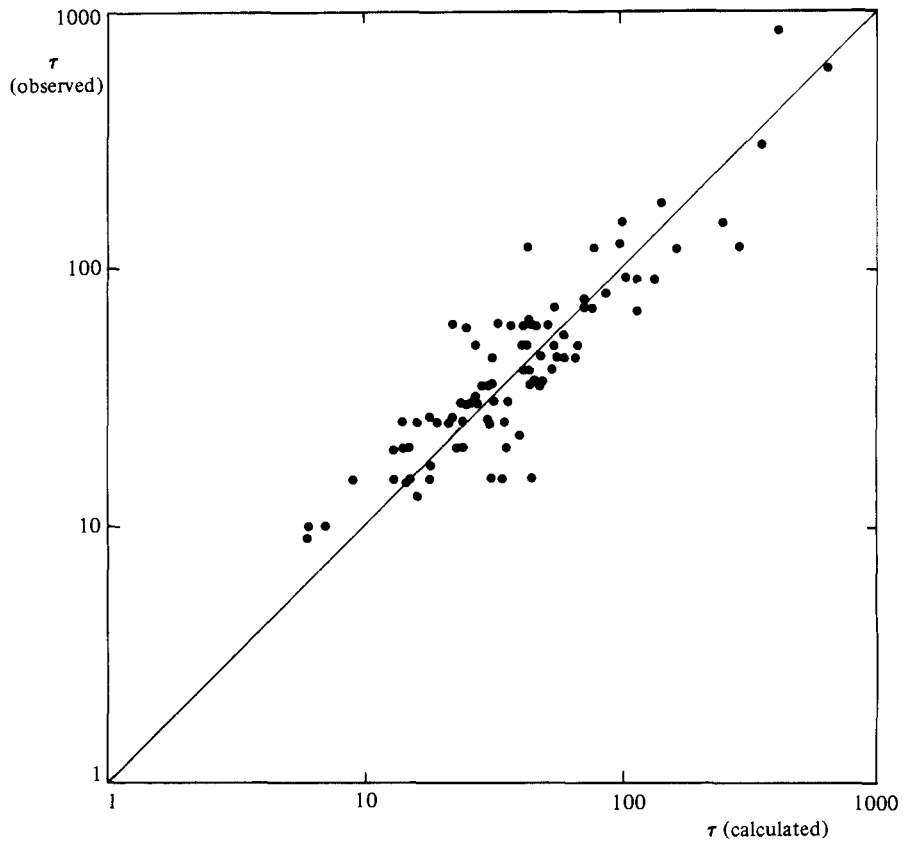

FIGURE 4. The observed spin-up time compared with the predicted value give by (4.10). The units are seconds and the straight line shows the theoretical value.

radius R, is plotted on figure 5 against the theoretical estimate given by (4.6), which is shown as the solid line. These figures contain all the observations from the four different tanks and over the full parameter ranges given in §2. The different symbols distinguish experiments with different depth ratios $\delta = h_0/H$, viz: ●, $0 < \delta \leqslant 0.1$; ○, $0.1 < \delta \leqslant 0.2$; ■, $0.2 < \delta \leqslant 0.3$; □, $0.3 < \delta \leqslant 0.4$; +, $0.4 < \delta \leqslant 0.5$; ×, $0.5 < \delta \leqslant 0.6$. With 3 exceptions the observed values of the bare-spot radius are smaller than predicted, with the discrepancy increasing with increasing δ. This is to be expected as the theory assumes that the upper layer is infinitely deep ($\delta = 0$) and ignores the motion in the upper layer.

5.2. *Upper-layer motion*

In the experiments the upper layer has finite depth and, in contrast with the assumptions of §4, significant upper-layer flow was observed. The motion in the upper layer was visualized by paper particles floating on the free surface, and streak photography permitted accurate determination of their velocities. Since the flow in the upper layer is approximately geostrophic, the free-surface motion is representative of the flow at lower levels in this layer.

During and immediately after the formation of the bare spot the flow is observed to be axisymmetric and, in the $f+\Delta f$ spun-up reference frame, anticyclonic. The

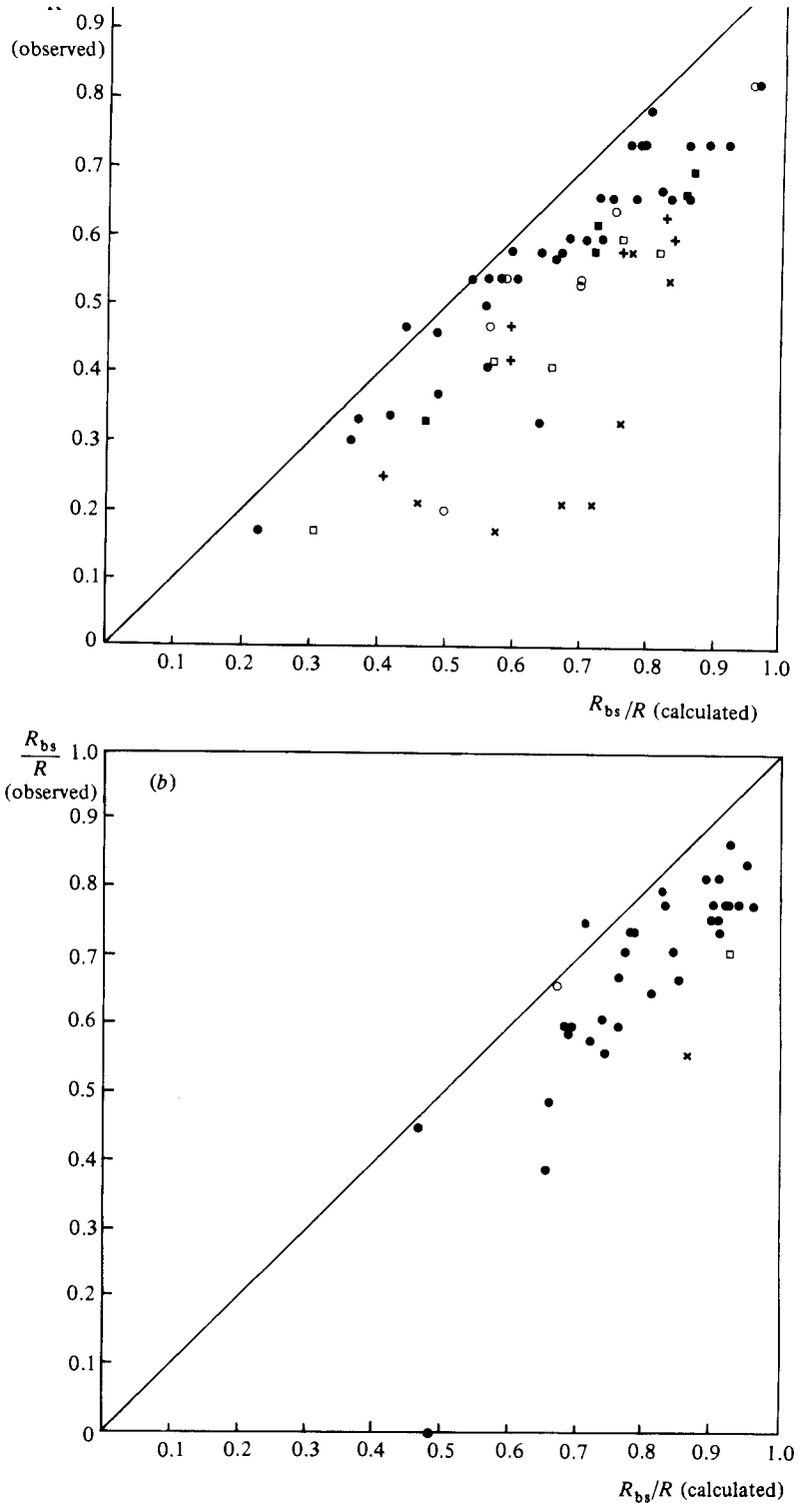

FIGURE 5. Observed values of the ultimate size of the bare spot R_{bs} non-dimensionalized by the tank radius R plotted against the predicted value given by (4.6). The data have been divided into those for the small tanks ($R = 12.1$ and 14.9 cm) in (a) and for the large tanks ($R = 44.7$ and 106.7 cm) in (b). The data are divided into different depth ratios: ●, $0 < \delta \leqslant 0.1$; ○, $0.1 < \delta \leqslant 0.2$; ■, $0.2 < \delta \leqslant 0.3$; □, $0.3 < \delta \leqslant 0.4$; +, $0.4 < \delta \leqslant 0.5$; ×, $0.5 < \delta < 0.6$. The predicted value for an infinite upper layer ($\delta = 0$) is shown by the straight line.

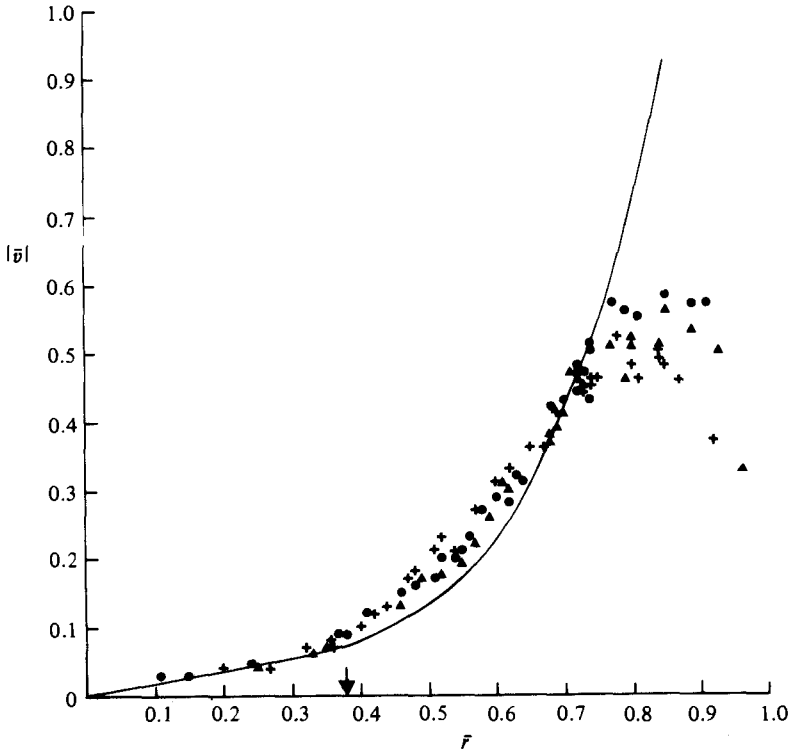

FIGURE 6. The magnitude of the (anticyclonic) azimuthal free-surface velocity $|\bar{v}|$ plotted against the dimensionless radius $\bar{r} = r/R$. The velocity $|\bar{v}|$ has been non-dimensionalized by the scale $\frac{1}{2}r\Delta f$. Three velocity profiles are shown corresponding to 102 (●), 152 (▲) and 234 (+) rotation periods after the start of the spin-up. In this experiment $R = 44.7$ cm, $h_0 = 1.8$ cm, $H = 20.9$ cm, $f = 2.02$ s^{-1}, $\Delta f = 0.11$ s^{-1} and $g' = 10$ cm s^{-2}. The position of the bare spot $\bar{r} = 0.38$ is indicated by the arrow. The solid line shows the velocity distribution obtained from conservation of potential vorticity in the upper layer.

strength of this anticyclonic, zonal flow is greatest above the ring of lower-layer fluid ($R_{bs} < r < R$), except for a region near the vertical wall of the tank where sidewall friction accelerates the flow. The flow above the bare spot is also anticyclonic, but in general is found to be considerably weaker.

Examples of the radial profile of azimuthal velocity $\bar{v}$ for the case of a small bare spot ($R_{bs}/R = 0.38$) are shown on figure 6. The velocity has been measured in the $f+\Delta f$ frame and non-dimensionalized by $\frac{1}{2}r\Delta f$, and is plotted against the non-dimensional radius $\bar{r} = r/R$. Thus if the upper layer were to remain at rest (as is assumed in §4) $|\bar{v}| = \bar{r}$, and the deviation of the observed profile from this line results from the finite depth of the upper layer and any frictional coupling between the layers. These profiles show that near the centre of the tank, over a region approximately equal to that of the bare spot, the velocity is approximately linear in r, corresponding to a (weak) solid-body rotation. Outside the bare spot the magnitude of the anticyclonic velocity increases more rapidly with radius, reaching a maximum near the sidewall, and then decreases again owing to the retardation of the anticyclonic flow by the sidewall boundary layer.

The three velocity profiles shown in figure 6 were measured at 102 (●), 152 (▲) and 234 (+) rotation periods after the start of the spin-up. Apart from the region

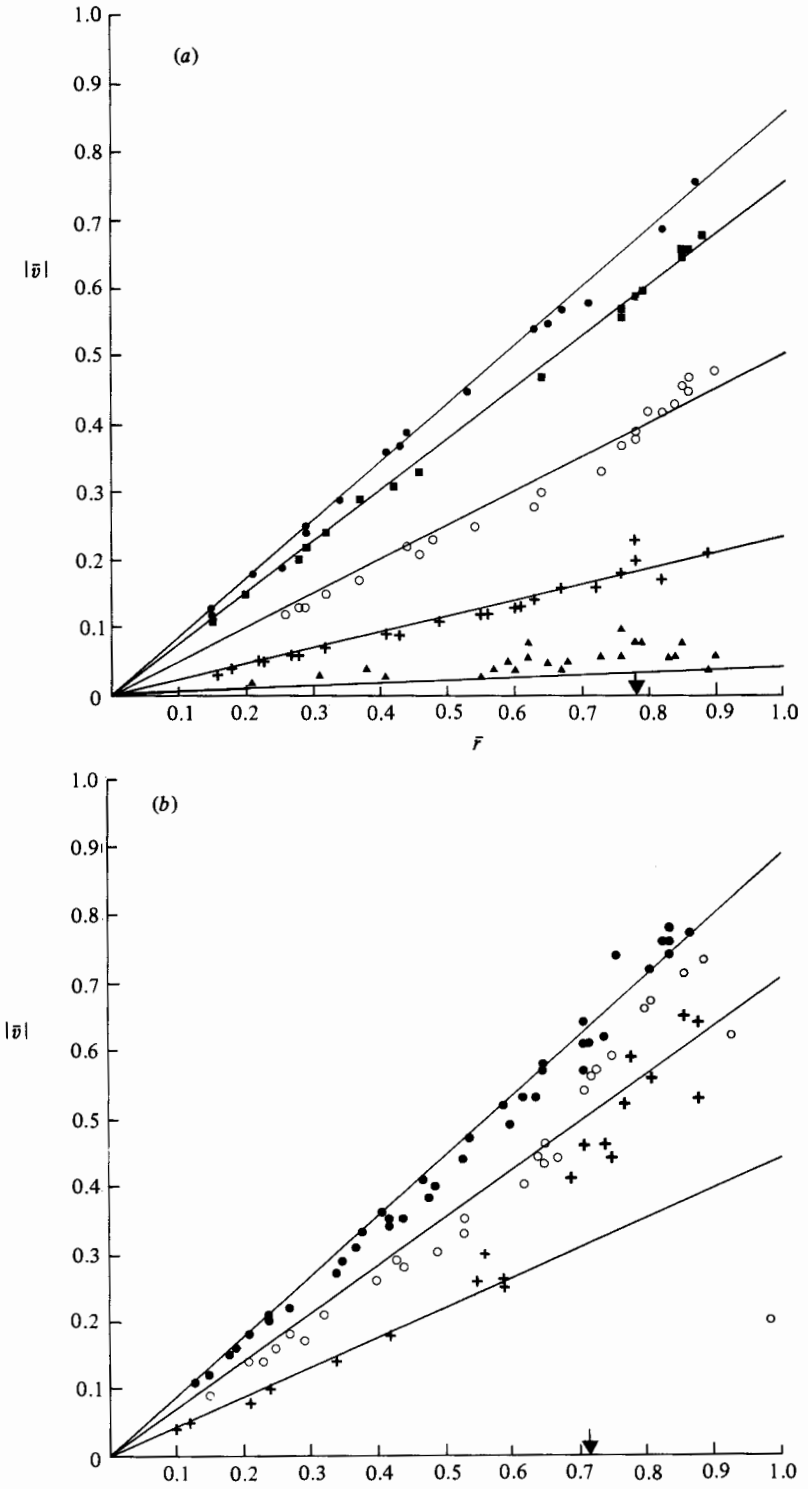

FIGURE 7. Profiles of the dimensionless azimuthal, free-surface velocity plotted against radius for two experiments with a large bare spot. The position of the edge of the bare spot is indicated by an arrow. Both experiments were in a tank with $R = 44.7$ cm and with $h_0 = 0.9$ cm, $H = 20.0$ cm and $g' = 10$ cm s^{-2}. In (*a*) $f = 2.07$ s^{-1}, $\Delta f = 0.072$ s^{-1}, and the profiles were measured at 7 (●), 13 (■), 33 (○), 67 (+) and 133 (▲) rotation periods from the start of the spin-up. In (*b*) $f = 0.63$ s^{-1}, $\Delta f = 0.26$ s^{-1}, and the profiles were measured at 4 (●), 11 (○) and 21 (+) rotation periods.

near the sidewall, the flow has an extremely slow time decay, indicating that the frictional coupling across the interface is very weak. (The homogeneous spin-up time based on the upper-layer depth is 24 revolutions.) On the other hand, over the region of the bare spot $0 \leqslant r \leqslant R_{\rm bs}$, where the upper layer is in direct contact with the tank bottom, we expect frictional effects to be important. In the example shown on figure 6 the area of the bare spot is small and the effect of bottom friction on the upper layer spin-up is weak.

In order to examine the influence of bottom friction on the upper layer, a number of experiments were performed in which a large bare spot was produced. Two typical examples of free-surface azimuthal velocity profiles (measured in the $f+\Delta f$ frame) are shown in figure 7. In both experiments $R_{\rm bs}$ lies in the range $0.7R < R_{\rm bs} < 0.8R$, and over the bare spot the velocities show an approximately linear dependence on r. However, in contrast with the velocity distributions shown on figure 6, the profiles on figure 7 show a rapid decay with time, indicating that the size of the bare spot is of major importance for the spin-up of the upper layer.

6. Finite upper layer

In the analysis given in § 4 two important simplifications of the real situation were made. These were the assumptions of an infinitely deep upper layer and the neglect of any frictional coupling across the interface between the two layers. We have already seen in § 5 that the latter assumption is quite reasonable, and we now turn our attention to the effects of a finite upper layer of depth H.

Assuming that no mixing occurs during spin-up, conservation of potential vorticity implies that the azimuthal velocity V in the upper layer is governed by

$$\frac{f}{H} = \frac{f+\zeta}{H+h_0-h(r)}, \tag{6.1}$$

where $\zeta = r^{-1}\,\mathrm{d}(rV)/\mathrm{d}r$ is the relative vorticity in the f-frame. The lower-layer motion is still $v = \frac{1}{2}r\,\Delta f$, and the depth of the lower layer $h(r)$ is given by

$$g'\frac{\mathrm{d}h}{\mathrm{d}r} = f(v-V)+\frac{v^2}{r}-\frac{V^2}{r}. \tag{6.2}$$

We non-dimensionalize these equations by scaling the velocity by $\frac{1}{2}R\,\Delta f$, the horizontal lengths by the tank radius R, and the vertical depths by the lengthscale f^2R^2/g'. The ratio of this latter scale with the depth of each layer is the Froude number for that layer. The dimensionless forms of (6.1) and (6.2) then become

$$\frac{\mathrm{d}h}{\mathrm{d}r} = \gamma(v-V)+\gamma^2\left[\frac{v^2}{r}-\frac{V^2}{r}\right], \tag{6.3}$$

$$\gamma\frac{1}{r}\frac{\mathrm{d}}{\mathrm{d}r}(rV) = F(h_0-h). \tag{6.4}$$

In these equations and for the remainder of this section all variables are dimensionless unless stated otherwise. Two dimensionless parameters appear in these equations: $\gamma = \frac{1}{2}\Delta f/f$, the incremental increase in rotation rate, and $F = f^2R^2/g'H$, the Froude number for the *upper* layer.

In the case when the upper layer is infinitely deep, $F = 0$, and so we seek a solution

to (6.3) and (6.4) as a perturbation expansion in powers of $F \ll 1$. Accordingly, we write

$$\left.\begin{aligned} h &= h^{(0)} + Fh^{(1)} + \ldots, \\ V &= V^{(0)} + FV^{(1)} + \ldots, \\ R_{\rm bs} &= R^{(0)} + FR^{(1)} + \ldots. \end{aligned}\right\} \tag{6.5}$$

We shall restrict our attention on the case where Δf is large enough to produce a bare spot. In this case we have the condition that

$$h(R_{\rm bs}) = 0, \tag{6.6}$$

and conservation of volume of the lower layer gives

$$\int_{R_{\rm bs}}^{1} h(r)\, r\, \mathrm{d}r = \tfrac{1}{2}h_0. \tag{6.7}$$

At leading order we simply recover the solution for an infinitely deep upper layer given in §4. In dimensionless variables this is

$$\left.\begin{aligned} V^{(0)} &= 0, \\ h^{(0)} &= A(r^2 - R^{(0)2}), \end{aligned}\right\} \tag{6.8}$$

where $A = \frac{1}{2}(\gamma+\gamma^2)$. The first term in the expansion for $R_{\rm bs}$ is given by (4.6), and in the present variables we have

$$R^{(0)} = \left[1 - \left(\frac{2h_0}{A}\right)^{\frac{1}{2}}\right]^{\frac{1}{2}}. \tag{6.9}$$

At $O(F)$ the upper-layer velocity satisfies

$$\gamma \frac{1}{r}\frac{\mathrm{d}}{\mathrm{d}r}(rV^{(1)}) = \left.\begin{cases} h_0 & (0 < r < R^{(0)}), \\ h_0 - A(r^2 - R^{(0)2}) & (R^{(0)} < r < 1), \end{cases}\right\} \tag{6.10}$$

and using (6.9) we find

$$V^{(1)} = \begin{cases} \dfrac{1}{2}\dfrac{h_0 r}{\gamma} & (0 < r < R^{(0)}), \\[2ex] \dfrac{1}{2}\dfrac{h_0}{\gamma}\left[r - \dfrac{(r^2 - R^{(0)2})^2}{r(1-R^{(0)2})^2}\right] & (R^{(0)} < r < 1). \end{cases} \tag{6.11}$$

This upper-layer velocity implies a correction to the lower layer given by

$$\frac{\mathrm{d}h^{(1)}}{\mathrm{d}r} = -\gamma V^{(1)}. \tag{6.12}$$

The boundary condition on $h^{(1)}$ is found by substituting (6.5) into (6.6) to give

$$h^{(1)}(R^{(0)}) = -2AR^{(1)}R^{(0)}, \tag{6.13}$$

and the solution to (6.12) is then

$$h^{(1)} = -\tfrac{1}{4}h_0(r^2 - R^{(0)2}) + \frac{h_0}{2(1-R^{(0)2})^2}\left\{\frac{r^4}{4} + \tfrac{3}{4}R^{(0)4} - r^2R^{(0)2} + R^{(0)4}\ln\frac{r}{R^{(0)}}\right\} - 2AR^{(0)}R^{(1)}. \tag{6.14}$$

In order to solve for $R^{(1)}$ we now apply the conservation of lower-layer volume given by (6.7). Substituting the series expansions (6.5) into (6.7) and using (6.8), we find,

after a few lines of algebra, that

$$\int_{R^{(0)}}^{1} h^{(1)}(r)\, r\, \mathrm{d}r = 0. \tag{6.15}$$

It is then straightforward to substitute (6.14) into (6.15) to obtain

$$R^{(1)} = -\frac{1}{96}\frac{(2-6R^{(0)2}+3R^{(0)4}(5+4\ln R^{(0)})-14R^{(0)6}+3R^{(0)8})}{R^{(0)}(1-R^{(0)2})} \tag{6.16}$$

Hence the (dimensionless) radius of the bare spot is

$$R_{\mathrm{bs}} = R^{(0)}(1-FQ(R^{(0)})+O(F^2)), \tag{6.17}$$

where

$$Q(x) = \frac{2-6x^2+3x^4(5+4\ln x)-14x^6+3x^8}{96x^2(1-x^2)} \quad (0 \leqslant x < 1). \tag{6.18}$$

The upper-layer velocity calculated from the conservation of potential vorticity and given explicitly in (6.11) can be compared with the velocity profiles presented in §5. Since the latter are measured on the $f+\Delta f$ frame a term $-\frac{1}{2}r\,\Delta f$ has been added to $V^{(1)}$, and the *observed* value of R_{bs} was used in (6.11). Over the region of the bare spot the velocity in the spun-up frame is $\frac{1}{2}(1-\Delta f/\delta f)\,\delta f r$; as observed, this is linear in r, and, provided that $\delta < \Delta f/f$, the motion is anticyclonic. This condition is always satisfied in our experiments when a bare spot is formed. The predicted upper-layer velocity with $R_{\mathrm{bs}} = 0.38$ is shown as the solid curve on figure 6, and except for the region near the sidewall there is good agreement with the observations. Thus when the bare spot occupies only a small fraction of the total area the calculation profile, which is strictly only valid immediately after the formation of the bare spot, describes the upper-layer velocity and shows that frictional effects are weak.

When the area of the bare spot is large, on the other hand, the inviscid calculation (6.11) is modified by bottom friction over the bare spot for times $t > \tau$, where τ is the time at which the bare spot reaches its ultimate size. It is reasonable to assume that the central part of the upper layer then starts to spin up in a manner similar to the spin-up of a single layer of homogeneous fluid. In that case the time-dependent swirl velocity $\bar{v}_*$ (measured in the $f+\Delta f$ frame) is (see Greenspan 1968, p. 168)

$$\bar{v}_*(\bar{r},t) = \frac{f+\Delta f}{\Delta f}\left[1-\frac{f}{f+\Delta f\,\mathrm{e}^{-2T_*}}\right]\bar{r}, \tag{6.19}$$

where $T_* = \frac{1}{2}fE_*^{\frac{1}{2}}t$ is the dimensionless time, with $E_* = 2\nu/fR^2$.

By analogy with this one-layer spin-up it is assumed for $t > \tau$ that the region over the bare spot ($0 \leqslant r \leqslant R_{\mathrm{bs}}$) of the upper layer spins up according to

$$\bar{v}(\bar{r},t) = \frac{f+\Delta f}{\Delta f}\left[1-\frac{f}{f+\Delta f\,\mathrm{e}^{-2T}}\right]\bar{v}_0(\bar{r},\tau) \quad (0 < r < R_{\mathrm{bs}}), \tag{6.20}$$

where

$$2T = f(t-\tau)\,E^{\frac{1}{2}}, \quad E = \frac{2\nu}{fR_{\mathrm{bs}}^2},$$

and $\bar{v}_0$ is the initial solid-body rotation as given by (6.11):

$$\bar{v}_0(\bar{r},\tau) = \left|\frac{\delta f}{\Delta f}-1\right|\bar{r}. \tag{6.21}$$

The solid lines drawn on figures 7 (a, b) are the velocity distributions according to the theoretical predictions (6.20) and (6.21) for $0 \leqslant r \leqslant R_{\mathrm{bs}}$, and they agree very well

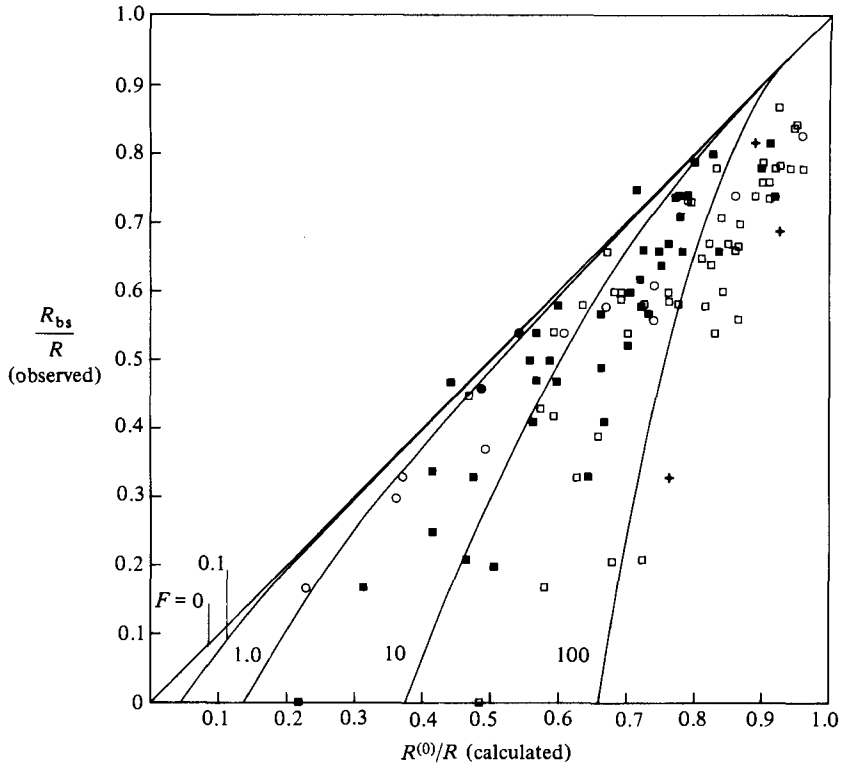

FIGURE 8. Observed values of the dimensionless bare-spot radius R_{bs}/R plotted against the value $R^{(0)}/R$ calculated when the upper layer is infinitely deep. The solid lines are the theoretical relationship (6.17) plotted for five different values of $F = f^2R^2/g'H$. The symbols correspond to different ranges of F: ●, $0 < F \leqslant 0.1$; ○, $0.1 < F \leqslant 1.0$; ■, $1.0 < F \leqslant 10$; □, $10 < F < 100$; +, $F > 100$.

with the experimental data. It can also be seen, especially in figure 7 (*b*), that the spin-up of the upper fluid for $R_{bs} < r < R$ takes place much more slowly than at smaller radii.

The effect of the finite upper-layer depth on the predicted size of the bare spot is shown on figure 8, where R_{bs} as given by (6.17) is plotted as the solid curves against $R^{(0)}$ for five values of the upper-layer Froude number $F = f^2R^2/g'H$ of $F = 0$ (infinite upper layer), 0.1, 1, 10 and 100. The correction to the infinite-depth case is largest for small values of the bare spot, consistent with the data. The symbol for each data point has been coded for the appropriate value of F for that particular experiment, and we seen that the data roughly accord with the calculated values.

A more direct comparison between experiment and theory is shown on figure 9, where the observed bare-spot radius is plotted against the predicted value given by (6.17). This figure shows there is quite good agreement between the predicted and measured values. The values of F in the experiments cover the range $0.1 \leqslant F \leqslant 246$, and although the series expansion (6.5) is strictly only valid for $F \ll 1$, no systematic trend between the differences between the predicted and observed values of the bare spot radius with F could be found. For large values of R_{bs}, the observed values tend to be smaller than predicted. This discrepancy may be due to the effects of sidewall friction on the upper-layer velocity near the outer boundary of the tank (see figure 6). For smaller bare spots, on the other hand, the theoretical values tend to be

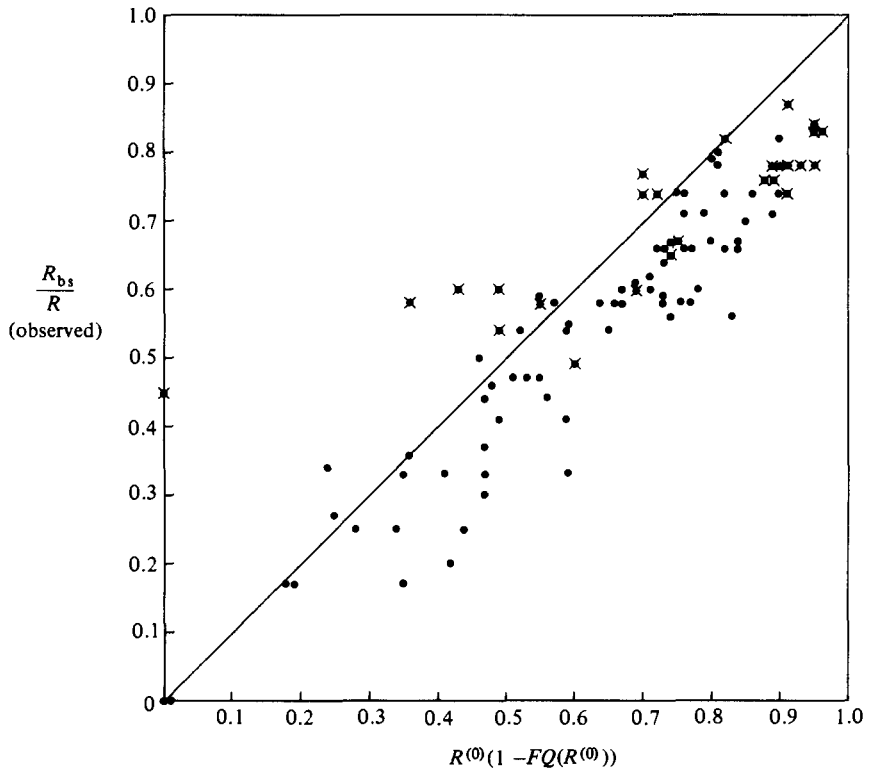

FIGURE 9. The observed bare-spot radius R_{bs}/R plotted against the predicted value $R^{(0)}(1-FQ(R^{(0)}))$ as given by (6.17). The points with crosses superimposed satisfy $T_w/T_s \geqslant 2$ (see (4.15)).

smaller than the observed ones, and in some cases the agreement is poor. We shall return to this comparison in §8.

7. Instability of the bare spot

As we briefly described in §3, the circular shape of the bare spot is distorted by the presence of waves which grow on the front surrounding the bare spot. The evolution of the bare spot as observed in the small tank ($R = 12.1$ cm) is illustrated on figure 3. Observations made in the large tank ($R = 44.7$ cm) show a similar wave patterns, although there are some differences. Ekman-layer instabilities were not observed in the large tank, and the structure of the backward breaking frontal waves is not so symmetrical. The frontal waves propagate anticyclonically as in the small tank, and their wavelength increases as they grow to large amplitude. However, the changes in wavelength are not as large as those changes observed in the small tank. These differences are thought to be due to the increased Reynolds numbers of the flow in the large tank and to increased interfacial slopes. Both of these effects are geometrical, and they lead to increased turbulence and interfacial mixing for the same incremental change in rotation rate (see (4.3) and (4.4)), as well as to more-pronounced baroclinic effects.

At large amplitude the motion in the upper layer associated with the frontal waves is observed to form regions of closed streamlines producing cyclonic vortices. A

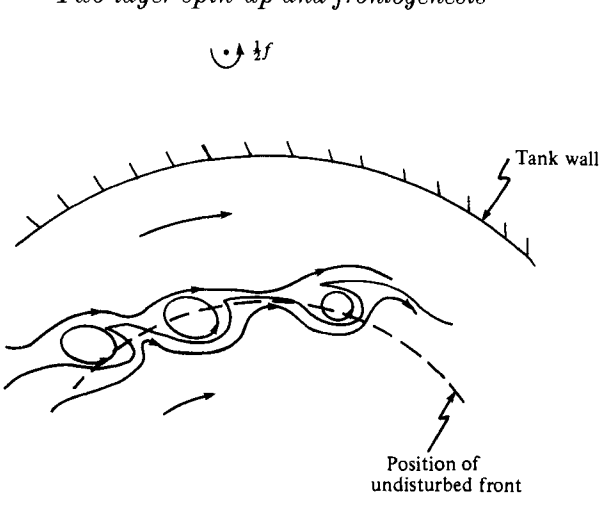

FIGURE 10. A diagrammatic representation of the upper-layer flow showing the formation of cyclonic eddies above the intrusions of the lower-layer fluid across the position of the undisturbed front into the bare spot. The arrows indicate the direction of flow.

schematic drawing showing the direction of motion is given on figure 10. The upper layer is observed to move anticyclonically (as shown by the solid arrows), with a greater speed on the stratified side of the front (see figure 6). The lower layer also moves anticyclonically, but much slower than the upper layer. Thus the *horizontal* shear between the two layers across the front is cyclonic, whilst the horizontal shear in the upper layer above the front is anticyclonic.

We shall first describe the motion of the upper layer, as this is the most readily observed. With this viewpoint in mind we shall (for definiteness) term the portion of the wave where the front recedes towards the wall as the wave crest, and the region where the lower layer intrudes onto the bare spot as the wave trough. As noted above the waves propagate anticyclonically (from left to right on figure 10) and so the crests break 'backwards' with the formation of closed cyclonic eddies in the troughs. Occasionally the motion in the crests pinches off to form closed streamlines – the vortices so formed are anticyclonic. This form of wave breaking with the production of cyclone–anticyclonic vortex pairs has been observed in waves at a free surface front (Griffiths & Linden 1981, 1982).

The motion in the lower layer is similar to that in the upper layer, with a cyclonic vortex being produced in each wave trough (still referring to the upper layer). Since the upper-layer wave trough is equivalent to a wave crest for the lower layer the presence of cyclonic circulation in the lower layer would seem to imply some asymmetry since the upper layer wave crests contain anticyclonic circulation. However, since the waves themselves are travelling anticyclonically more rapidly than the lower layer, *relative to the waves* the lower layer flow is reversed. Consequently, in a frame of reference moving with the waves the motion in both layers is symmetrical with anticyclonic vorticity being concentrated in the wave crests and cyclonic vorticity in the troughs. One difference between the two layers is reflected in the absence of the sharp cusp on the lower-layer crests which is present on upper-layer crests. This may be the result of increased frictional drag on the lower layer inhibiting the motion of the lower layer.

At very large amplitude the waves exhibit significant radial and azimuthal

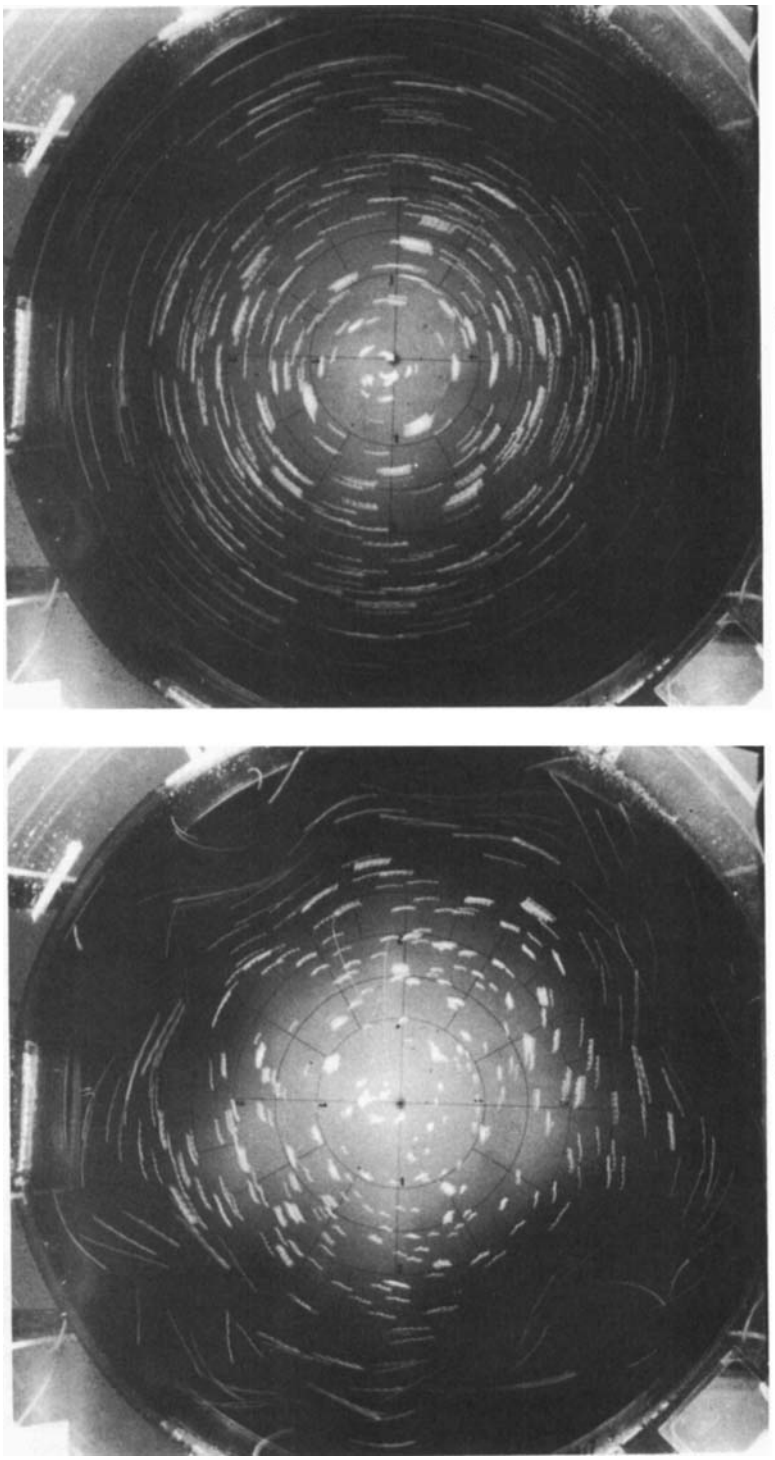

FIGURE 11 (*a*, *b*). For caption see facing page.

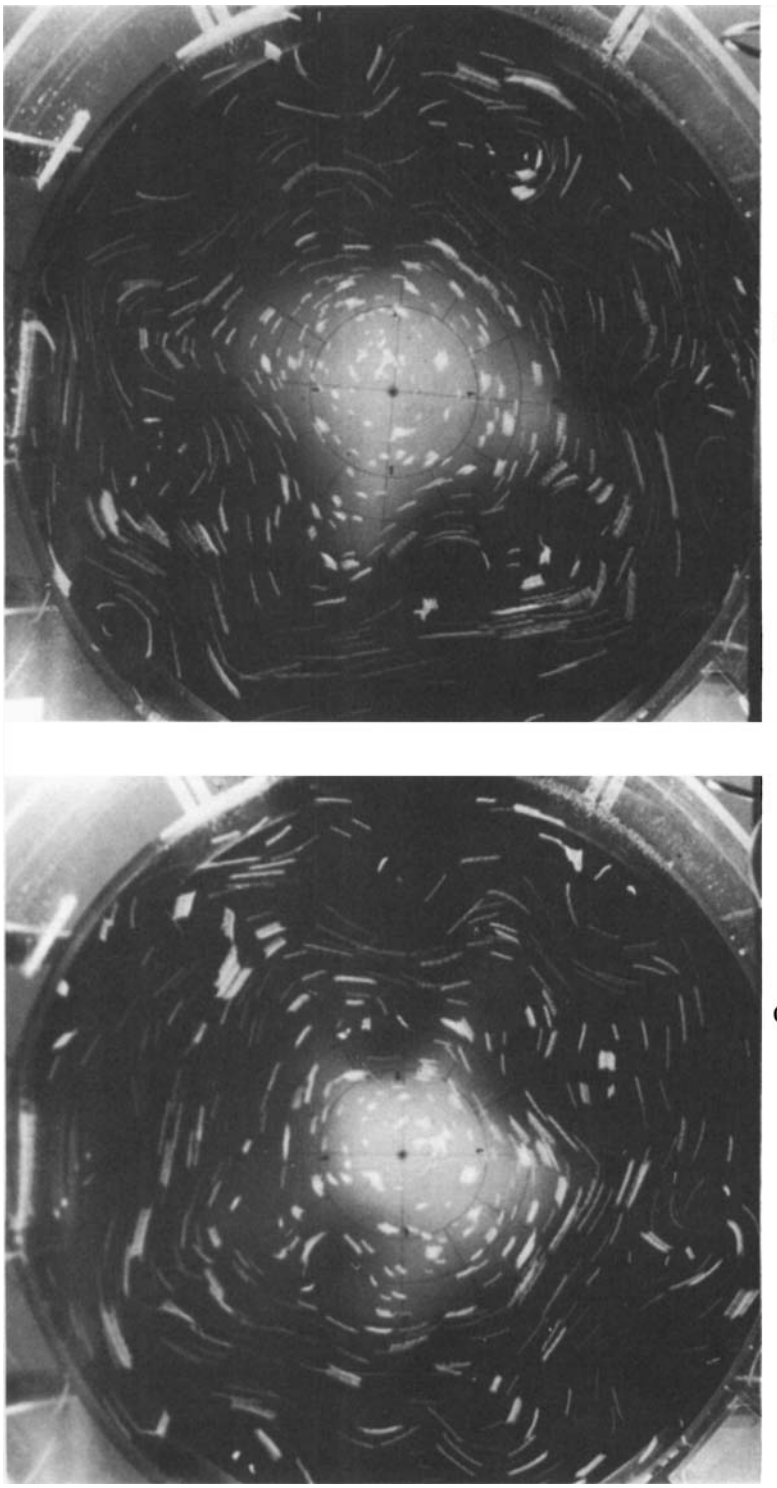

FIGURE 11. A set of streak photographs showing the growth of baroclinic waves on the interface in a case when no bare spot is formed during spin-up. The initially circular flow (*a*) is unstable to azimuthal waves with zonal wavenumber $n = 8$ (*b*, *c*, *d*). The photographs are 8 s exposures and were taken at 19, 44, 70 and 84 revolutions respectively. In this experiment $R = 44.7$ cm, $h_0 = 2.0$ cm, $H = 5.0$ cm, $f = 1.85\ \mathrm{s}^{-1}$, $\Delta f = 0.34\ \mathrm{s}^{-1}$ and $g' = 10\ \mathrm{cm\ s}^{-2}$.

motions. These cause regions of the tank bottom under the bare spot to be temporarily covered by lower-layer fluid as the waves pass by. Subsequently the bottom is again exposed to the upper layer. These are isopycnal motions which allow upper-layer fluid to be in contact with the bottom and then swept up over the interface, and they provide a potential source of energy for transporting material off the bottom into the upper layer (see Lambert *et al.* 1983).

If, on the other hand, the change in rotation rate is not sufficiently large the descent of the interface in the centre of the tank is observed to cease before a bare spot is formed. An example of this case is shown on figure 11, which is a series of streak photographs showing the motion of small particles on the free surface. The variation in the depth of the lower layer is shown by the gradation in the tone due to the dye in the lower layer. (Although the central region is shallow as indicated by the light colour, the interface never intersected the bottom.)

The initially circular flow is unstable with waves developing on the sloping interface. In this example the azimuthal wavenumber $n = 8$. The upper-layer flow is anticyclonic (clockwise), and the closed eddies which form are all cyclonic and, as is the case with the frontal waves, associated with the lower-layer crests. This can be seen from the presence of a relatively deep region of the lower layer underneath the cyclones as indicated by the darker concentration of dye. The closed circulations are observed to form near the outer wall of the tank where the interface slope is steepest (see (4.4)) and where there is cyclonic shear due to the presence of a sidewall boundary layer (see figure 6). The cyclones propagate towards the centre of the tank remaining above the wave crests (see figures 11*c–d*).

These observations reveal many similarities with waves observed on the fronts at the free surface by Griffiths & Linden (1981, 1982). These authors identified two energy sources for the waves at surface fronts: kinetic energy associated with the horizontal shear across the interface and potential energy associated with the horizontal density gradients. Both of these energy sources, which we shall refer to as barotropic and baroclinic respectively, are present in the current experiments.

The simplest model for the baroclinic instabilities is to consider two uniform layers moving with constant, but different, velocities in a rotating channel. This model was first discussed by Phillips (1954) and later extended by Pedlosky (1970). In this quasi-geostrophic approximation where interface slopes are small, they show that in the absence of friction growing modes will occur whenever the Froude number $\mathscr{F} = f^2L^2/g'h_0$ exceeds a critical value $\mathscr{F}_c$. Here L is the width of the channel and h_0 the depth of, say, the lower layer. The critical value $\mathscr{F}_c$ depends on $\delta = h_0/H$, the ratio of the layer depths, and at the critical value the marginally unstable waves have infinitely long downstream wavelength. On the other hand, when there is viscous dissipation in Ekman layers at the interface and at the upper and lower boundaries they showed (for $\delta = 1$) that these long waves are damped. In addition to exceeding a critical Froude number it is also necessary to exceed a critical shear between the two layers to produce growing waves. Griffiths & Linden (1981) have extended this linear stability analysis to the case of unequal layer depths. They find that both the magnitude of the critical shear and $\mathscr{F}_c$ decrease as δ increases. The wavenumber k of the marginally unstable mode is a weak function of the depth ratio, but for a fixed Froude number k increases as δ increases.

In order to compare our observations with these calculations we shall ignore the effects of the circular geometry and define the Froude number $\mathscr{F} = f^2L^2/g'h_0$, where h_0 is the depth of the lower layer before spin-up and $L = R - R_{bs}$ is the width of the annular region outside the bare spot. Consider now the sequence of events immediately

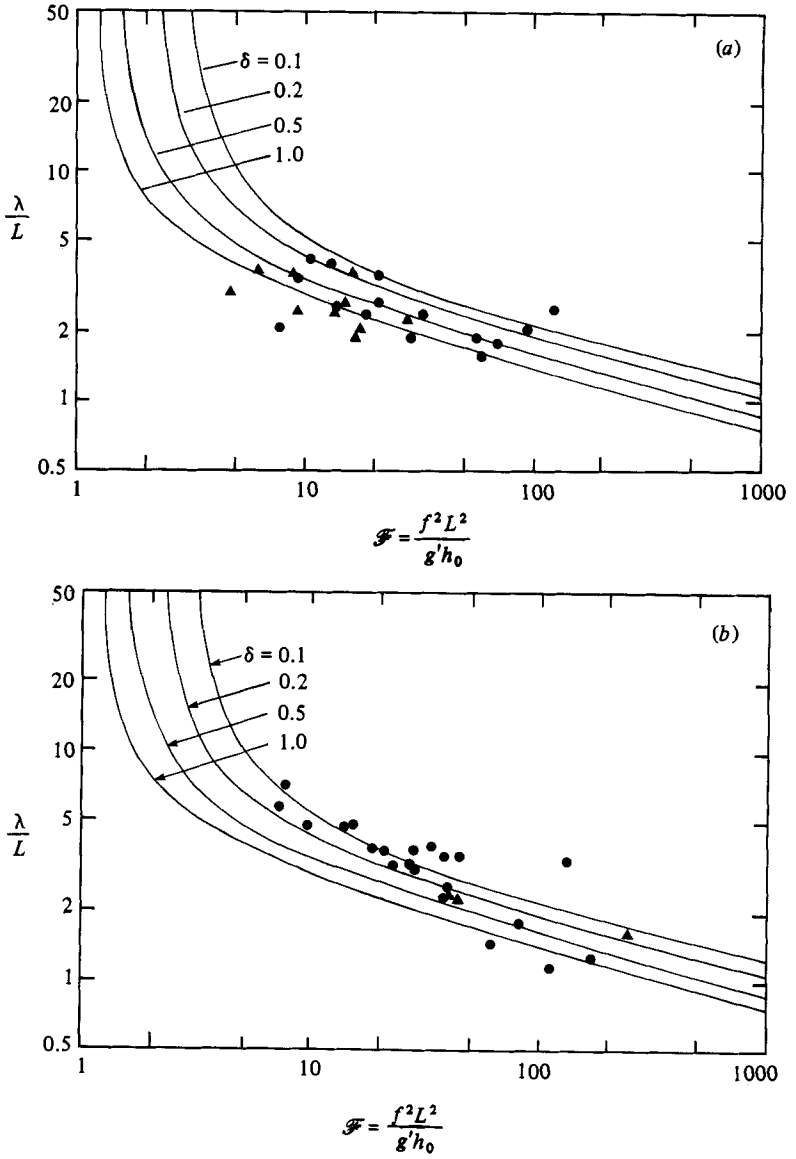

FIGURE 12. The zonal wavelength of the frontal instabilities non-dimensionalized by the width of the lower layer $L = R - R_{bs}$ plotted against the Froude number $\mathscr{F} = f^2L^2/g'h_0$. The solid curves are taken from theoretical estimates of the marginally stable wavelengths obtained by Griffiths & Linden (1981) for different values of the depth ratio δ. The circles correspond to experiments in which $\delta \leqslant 0.1$ and the triangles for $\delta > 0.1$, and the data have been plotted separately for the large tank ($R = 44.7$ cm) in (*a*) and the small tank ($R = 12.1$ cm) in (*b*).

following the spin-up of the cylinder. Azimuthal motion is transmitted to the lower layer whilst the interface is descending, and before the interface intersects the bottom a vertical shear exists across the interface. During this time the Froude number takes its maximum value with $L = R$, the radius of the tank, and is typically highly supercritical with values of $\mathscr{F} \geqslant 10$. Under these conditions the quasigeostrophic theory would lead us to expect, in the absence of dissipation, growth of baroclinic waves within a few rotation periods (Griffiths & Linden 1982). We never observed

the growth of non-axisymmetric disturbances before the formation of the bare spot had occurred, a process which usually took many rotation periods (see figure 4).

We conclude, therefore, that dissipation in Ekman layers inhibits the growth of the baroclinic waves until a critical shear is exceeded. The shear across the interface increases as the lower layer spins up and is a maximum once the bare spot has reached its greatest diameter, and it is soon after this time that the frontal waves are observed. Once the critical shear is exceeded, baroclinic waves begin to grow with a given wavenumber as determined by Griffiths & Linden (1981). Comparison between the present observations and these theoretical predictions are shown on figures 12(*a–b*). The dimensionless wavelength λ/L was calculated from the zonal wavenumber n according to

$$\frac{\lambda}{L} = \frac{2\pi R}{nL}.$$

As was noted in §3, the zonal wavelength of the frontal waves was observed to increase during a given experiment. There is therefore some ambiguity in the value of λ used in figure 12, and we have chosen the value that corresponds to the waves that grew to sufficiently large amplitude that closed streamlines were formed. Shorter wavelengths are produced by Ekman-layer instability (see figure 3*a*) and Kelvin–Helmholtz instability on the moving front. These instabilities were generally of short duration, and these have not been included on figure 12. At much longer times as the size of the bare spot diminishes, some waves were observed to decay presumably by bottom friction, and this transition is not included on figure 12.

The agreement between the theoretical curves and the data on figure 12, together with the qualitative similarities described earlier, indicate that these waves on the bare-spot front have essentially the same characteristics as those observed on surface fronts by Griffiths & Linden (1981). Thus we conclude that these waves obtain a significant fraction of their energy from the potential energy stored in the sloping interface via baroclinic instablity. This conclusion is supported by the observation that the growth rate of the waves increased with the depth ratio δ.

8. Summary and conclusions

In this paper we have presented a theoretical and experimental investigation of the spin-up of a two-layer fluid in a cylinder. We have concentrated on the case in which the upper surface is free and where the change in rotation rate is sufficiently large so that suction into the bottom Ekman layer causes the interface to descend in the centre of the tank and intersect the bottom. Thus in a circular region centred on the axis of the tank (and the axis of rotation) the lower layer is removed by the spin-up and upper-layer fluid is in direct contact with the bottom. We call this region the 'bare spot'.

Observations of the formation of the bare spot were made, and its ultimate size was compared with theoretical calculations based on the assumption that the bare spot stopped growing once the lower layer acquired the new angular velocity of the container. It was further assumed that there was no frictional coupling across the interface between the two layers. This latter assumption was supported by direct observations of the velocity of the upper layer, and by the fact (see §2) that in all the experiments the interface thickness exceeded the Ekman-layer thickness. Reasonably good agreement was obtained with the observations by theoretical calculations involving a perturbation expansion in the parameter $F = f^2R^2/g'H$, the Froude number for the upper layer.

As was pointed out in §4, the assumption that the lower layer acquires the increased angular velocity of the container will only be valid for sufficiently small containers. As the horizontal scale of the layer increases, the time taken for information to propagate in from the sidewall exceeds the (homogeneous) spin-up time of the lower layer, and flow in the Ekman layer will continue to accumulate fluid near the outer boundary of the tank. Under these circumstances we would expect the size of the bare spot to exceed the value predicted by (6.17).

We established in §4 that the relevant ratio of timescales is $T_w/T_s = \nu^{\frac{1}{2}} f^{\frac{1}{2}} R/g'^{\frac{1}{2}} h_0^{\frac{3}{2}}$ as given by (4.15), and we have marked on figure 9 those experiments in which $T_w/T_s \geqslant 2$ (thus allowing for two spin-up times). For values of $R_{bs}/R < 0.7$ almost all the experiments in which the observed size of the bare spot significantly exceeds the theoretical prediction have values of $T_w/T_s \geqslant 2$. At larger values of R_{bs}/R the observed values tend to be smaller than the theory predicts. This is probably a direct influence of the wall as the edge of the bare spot would be within one or two Rossby radii (based on the lower-layer depth) of the outer boundary of the tank.

We therefore conclude that the size of the bare spot is adequately given by the leading order in the perturbation expansion given by (6.17), provided that the tank radius is small enough for information from the outer boundary to propagate inwards and cause the lower layer to spin up. At larger values of R the central portion of the lower layer does not spin up, and Ekman-layer transport continues, thereby producing a larger bare spot.

At larger times the front at the edge of the bare spot was observed to become unstable to baroclinic frontal waves. These waves grow to large amplitude and then 'break' to form regions of closed streamlines in the upper layer. These waves severely distort the circularity of the bare spot, and as they propagate regions at the tank bottom are alternately brought into contact with the upper and then the lower layer. The flow patterns produced by these waves have qualitatively similar features to those produced at a front at the free surface, and the wavelengths agree with theoretical calculations of baroclinic instability including dissipation in Ekman layers (Griffiths & Linden 1981).

In this paper we have concentrated on the initial stages of the spin-up of the two-layer system. The final approach to the ultimate state in which both layers acquire the new angular velocity of the container has not been examined quantitatively and must remain the subject of a further study. What does seem clear though is that the frontal waves will play an important role in this process, particularly when wave breaking occurs and regions of closed streamlines form. These vortices move across the frontal boundary and provide an efficient mechanism for removing potential energy from the front and transporting lower-layer fluid into the interior.

We have shown that, when the lower layer is shallow, Ekman suction can be sufficient for frontogenesis. The experiment is not a direct model of the benthic boundary layer underneath an anticyclonic mesoscale eddy but there are sufficient similarities to the oceanic case to support the view proposed by Armi & D'Asaro (1980) that benthic fronts can be formed in such a situation. In this way the sea bottom is exposed to water from above the benthic boundary layer, and the presence of baroclinic instabilities on the front provides an important mechanism for transporting water on and off the exposed region. As Lambert *et al.* (1983) suggest, this process may be important for removing material from the oceanic sediments.

This work has benefited from numerous stimulating conversations with Melvin Stern, and we are grateful to David Smeed for comments on an earlier draft of this

paper. One of us (G.J.F. v.H.) gratefully acknowledges support from the Netherlands Organisation for the Advancement of Pure Research (Z.W.O.).

REFERENCES

ARMI, L. 1978 Some evidence for boundary mixing in the deep ocean. *J. Geophys. Res.* **83**, 1971–1979.

ARMI, L. & D'ASARO, E. 1980 Flow structures of the benthic ocean. *J. Geophys. Res.* **85**, 469–484.

BAKER, D. J. 1968 A demonstration of magnification of dynamic topography at the thermocline *J. Mar. Res.* **26**, 283–285.

BENTON, E. R. & CLARK, A. 1974 Spin-up. *Ann. Rev. Fluid Mech.* **6**, 257–280.

BUZYNA, G. & VERONIS, G. 1971 Spin-up of a stratified fluid: theory and experiment. *J. Fluid Mech.* **50**, 579–608.

EKMAN, V. W. 1905 On the influence of the earth's rotation on ocean currents. *Ark. Mat. Astr. Fys.* **2**, 1–52.

GREENSPAN, H. P. 1968 *The Theory of Rotating Fluids.* Cambridge University Press.

GREENSPAN, H. P. & HOWARD, L. N. 1963 On time-dependent motion of a rotating fluid. *J. Fluid Mech.* **17**, 385–404.

GRIFFITHS, R. W. & LINDEN, P. F. 1981 The stability of buoyancy-driven coastal currents. *Dyn. Atmos. Oceans* **5**, 281–306.

GRIFFITHS, R. W. & LINDEN, P. F. 1982 Laboratory experiments on fronts. Part 1. Density driven boundary currents. *Geophys. Astrophys. Fluid Dyn.* **19**, 159–187.

HOLTON, J. R. 1965 The influence of viscous boundary layers on transient motions in a stratified rotating fluid. Part 1. *J. Atmos. Sci.* **22**, 402–411.

LAMBERT, C. E., LINDEN, P. F., LOWENTHAL, D. & STERN, M. E. 1983 Benthic fronts and the global excess Radon distribution. *Geophys. Astrophys. Fluid Dyn.* **25**, 309–315.

LIGHTHILL, M. J. 1978 *Waves in Fluids*, Cambridge University Press.

PEDLOSKY, J. 1967 The spin-up of a stratified fluid. *J. Fluid Mech.* **28**, 463–479.

PEDLOSKY, J. 1970 Finite amplitude baroclinic waves. *J. Atmos. Sci.* **27**, 15–30.

PHILLIPS, N. A. 1954 Energy transformations and meridional circulations associated with simple baroclinic waves in a two-level quasi-geostrophic model. *Tellus* **6**, 273–286.

WALIN, G. 1969 Some aspects of time-dependent motion of a stratified rotating fluid. *J. Fluid Mech.* **36**, 289–307.